



## OPEN ACCESS

## EDITED BY

Hu Li,  
Sichuan University of Science and  
Engineering, China

## REVIEWED BY

Ruyue Wang,  
State Key Laboratory of Shale Oil and Gas  
Enrichment Mechanisms and Efficient  
Development, China

Jingshou Liu,  
China University of Geosciences  
Wuhan, China

Shun He,  
Southwest Petroleum University, China  
Md. Bazlar Rashid,  
Geological survey of Bangladesh, Bangladesh

## \*CORRESPONDENCE

Xiangdong Peng,  
✉ 161972010013@nepu.edu.cn

RECEIVED 15 March 2025

ACCEPTED 15 May 2025

PUBLISHED 30 May 2025

## CITATION

Yang L, Peng X, Hu Y and Liu A (2025) Shale lithofacies mechanical differences from tectonic-digenetic coupling and their response to hydraulic fracture network propagation.  
*Front. Earth Sci.* 13:1594244.  
doi: 10.3389/feart.2025.1594244

## COPYRIGHT

© 2025 Yang, Peng, Hu and Liu. This is an open-access article distributed under the terms of the [Creative Commons Attribution License \(CC BY\)](https://creativecommons.org/licenses/by/4.0/). The use, distribution or reproduction in other forums is permitted, provided the original author(s) and the copyright owner(s) are credited and that the original publication in this journal is cited, in accordance with accepted academic practice. No use, distribution or reproduction is permitted which does not comply with these terms.

# Shale lithofacies mechanical differences from tectonic-digenetic coupling and their response to hydraulic fracture network propagation

Liyan Yang<sup>1</sup>, Xiangdong Peng<sup>1\*</sup>, Ying Hu<sup>2</sup> and Anan Liu<sup>3</sup>

<sup>1</sup>School of Earth Sciences, Northeast Petroleum University, Daqing, Heilongjiang, China, <sup>2</sup>Geological Logging Company (Geological Research Institute) of Daqing Oilfield Co., Ltd., Daqing, China, <sup>3</sup>College of Continuing Education, Northeast Petroleum University, Daqing, Heilongjiang, China

Fracture propagation modes in shale formations exhibit significant variations across different lithofacies during tectonic deformation and hydraulic fracturing. Understanding how the mechanical properties of these lithofacies influence fracture network development is crucial for effective shale reservoir stimulation. This study investigates the organic-rich Wufeng–Longmaxi Formation shale in the southern Sichuan Basin. Lithofacies were classified, and their mechanical properties analyzed, focusing on stress–strain behavior and energy accumulation/release characteristics under varying stress conditions. The study also examines the fracturing behavior of single and stacked lithofacies combinations. The findings reveal five primary lithofacies in the Lower Longmaxi (Long-1) submember of the study area. Under uniaxial compression, samples from different lithofacies predominantly fail through tensile splitting, exhibiting linear elastic energy accumulation and vertical splitting fractures. Under triaxial compression, the elastic deformation phase shortens, with increased energy dissipation during plastic deformation; shear fractures become the dominant failure mode. Among the lithofacies, siliceous shale exhibits the largest stress drop and highest ratio of released elastic energy, leading to the most intense failure. Due to its brittleness, siliceous shale undergoes planar fracture propagation in stress-unloading zones. Laminated calcareous–siliceous shale demonstrates fracture propagation capacity second only to siliceous shale, while clay-rich siliceous shale shows the weakest fracture development. Hydraulic fracturing in a stacked sequence of thinly laminated siliceous shale and clay-rich siliceous shale is significantly influenced by bedding planes acting as “stress barriers.” Fractures propagating upward exhibit stepped, staircase-like growth and branching, forming a complex fracture network characterized by short fracture segments, numerous branches, complex morphologies, and strong lateral connectivity. In contrast, combinations of massive siliceous shale and massive clay-rich siliceous shale (with minimal bedding) facilitate vertical stress transmission, resulting in simpler fractures that are fewer in number, longer, and more planar. These insights provide valuable guidance for identifying sweet spots and

optimizing stimulation strategies in shale formations with varying lithofacies combinations.

#### KEYWORDS

fracture network propagation, lithofacies combination, hydraulic fracturing, mechanical properties, organic-rich shale, Wufeng-Longmaxi formation

## 1 Introduction

Fault and fracture characteristics within shale layers vary with lithofacies (Wang R. et al., 2023). During tectonic deformation, siliceous shale tends to develop steeply dipping, densely spaced faults and fractures, whereas more ductile clay-rich shale develops faults at lower dips and absorbs stress, resulting in fewer and smaller fractures (Fan et al., 2020; 2024; Zhao et al., 2023; Liu et al., 2024b). These mechanical-property-driven differences are likewise evident during artificial reservoir stimulation (hydraulic fracturing) of shale reservoirs. Due to their low porosity, low permeability, and poor pore connectivity, shale reservoirs require large-scale hydraulic fracturing (typically via horizontal wells with multistage fracturing) for effective development (Zheng et al., 2020; Wu et al., 2022; Sun et al., 2023). The success of shale gas development hinges on creating extensive fracture networks through high-volume, high-sand hydraulic fracturing. In China's marine shales, the target intervals are often organic-rich siliceous shale, primarily because hydraulic fracturing in these brittle, silica-rich shales can generate a more complex fracture network that connects more isolated matrix pores (Li H. et al., 2024; Wang Y. Y. et al., 2024). In deep-water sedimentary shales, higher brittleness often correlates with better gas content, and correspondingly these intervals yield superior fracturing results in production. In recent years, studies have underscored that lithofacies composition and mechanical properties significantly influence fracture development and complexity. However, the integrated influence of tectonic stress history and diagenetic alteration on lithofacies-specific mechanical traits and fracture propagation is not fully understood (Zhang et al., 2022; Li Y. et al., 2024). We quantify how variations in diagenetic mineralogy and tectonic deformation across lithofacies translate into differences in rock strength and brittleness, and how these differences control hydraulic fracture network morphology. By establishing this linkage between geological evolution and fracturing behavior, our work advances theoretical understanding of fracture mechanics in heterogeneous reservoirs and offers practical guidance for optimizing hydraulic fracturing in complex shale formations.

In shale volumetric fracturing engineering, the complexity of fracture development is influenced by both geological and engineering factors, with geological factors serving as the fundamental determinants of fracturing effectiveness. Existing studies have confirmed that during the fracturing transformation of shale reservoirs, as the horizontal maximum principal stress difference increases, fractures tend to propagate in a specific direction, forming longer fractures that are relatively simple and have a smaller transformed volume. Simultaneously, the fracture propagation during hydraulic fracturing generally exhibits a “soft-to-hard” avoidance pattern (Li et al., 2025).

The greater the brittleness of the rock, the more fractures tend to propagate in a “planar” manner, resulting in shorter

fractures but with more diverse propagation directions, leading to a larger transformed reservoir volume. Hou et al. (2023) utilized hydraulic fracturing simulation to indicate that fracture propagation morphology is influenced by net pressure, horizontal maximum principal stress difference, and the orientation of natural fractures. When the relative net pressure exceeds 2 MPa and the horizontal maximum principal stress difference is less than 4 MPa, under the influence of the local stress field near the tip of natural fractures, fracture connectivity becomes increasingly complex, with greater propagation distances and larger scales of communication with natural fractures. Additionally, they noted that shales with high brittleness are more prone to fracture formation, and the simulated fracture morphology is also more complex.

Shale lithofacies reflect differences in diagenetic minerals, organic matter content, bedding, fossils, and other features. Previous studies on marine shales indicate that different lithofacies show distinct rock mechanical properties and gas-bearing characteristics (Chen et al., 2023; El-Sayed et al., 2024; Jiang et al., 2025). These mechanical differences lead to variations in fracture propagation modes and extents under stress (Yu et al., 2024b). During reservoir stimulation, the initiation and propagation of hydraulic fractures differ markedly among lithofacies. Additionally, variations in bedding and natural fracture density between lithofacies create natural discontinuities that make the rock mechanically heterogeneous. As a propagating fracture crosses such discontinuities, the weak cementation of bedding planes exhibits varying resistance to crack propagation. In the direction parallel to the bedding, the resistance to crack extension is relatively weak, whereas in the direction perpendicular to the bedding, the resistance is stronger. Consequently, the stress may dissipate, deflect, or bifurcate. In fracturing operations, these natural planes can divert fluid flow, alter fracture orientation and length, and result in more complex fracture network systems (Zhou, 2023). At the same time, shale lithofacies are closely linked to shale's hydrocarbon generation, reservoir quality, and gas content. Essentially, hydraulic fracturing creates artificial fractures to connect isolated pores and enhance shale gas flow. Therefore, researching the mechanical properties of different lithofacies and their fracturing responses is of practical significance for efficient shale reservoir stimulation.

In this paper, the Wufeng-Longmaxi Formation shale of the southern Sichuan Basin is selected as the study subject. Based on lithofacies classification from a geological and development perspective, we establish a lithofacies classification scheme and conduct rock mechanics experiments to evaluate brittleness and stress-strain/energy evolution for each lithofacies. We then summarize the fracturing responses of different single-facies and multi-facies combinations. Considering the actual vertical stacking of lithofacies in the formation, we analyze how lithofacies

differences affect hydraulic fracture network propagation. The specific objectives of this study are: (1) to systematically classify the shale lithofacies in the Wufeng–Longmaxi Formation considering their tectonic and diagenetic histories; (2) to quantify the mechanical differences (strength, brittleness, energy release) among these lithofacies through laboratory testing; and (3) to investigate how these differences affect hydraulic fracture propagation patterns using sequential fracturing experiments. By achieving these objectives, the research not only advances fundamental understanding of how geological history shapes fracture mechanics, but also has practical significance for unconventional oil and gas development both in China and internationally. In particular, our findings provide guidance for identifying sweet spots and optimizing hydraulic fracturing designs in heterogeneous shale reservoirs, thereby supporting the efficient exploitation of unconventional resources globally.

## 2 Geological setting

The study area is located in southern Sichuan Basin, on the northwestern margin of the Upper Yangtze Platform. Tectonically, it lies in the gently folded southern Sichuan region at the southern end of the Yongchuan broom-shaped structure, near the junction of the central Sichuan paleo-uplift gentle slope, southwestern Sichuan low-fold zone, and southern Sichuan paleo-depression (Figure 1) (Feng et al., 2020; Xiong et al., 2025). Influenced by the Huayingshan strike-slip fault and Qijiang fault, the study area exhibits pronounced wrench-fault structural characteristics. The structural axes trend NE–NNE, showing a “converging in the north, diverging in the south” pattern, with well-developed NE and NNE fault systems (He X. Y. et al., 2025; He S. et al., 2025).

During the Late Ordovician, following the end of the glaciation, global climate warmed and sea level rose, leading to a widespread transgression in southern Sichuan. The depositional water depth increased, and, constrained by surrounding paleo-uplifts (Qianzhong, central Sichuan, and Jiangnan–Xuefeng uplifts), seawater circulation became restricted. This resulted in large, laterally continuous stratified anoxic water bodies and deposition of a regionally extensive organic-rich shale. The shale thins gradually toward the central Sichuan Basin. Due to fluctuating sediment supply and water conditions during the Wufeng–Longmaxi deposition, the lithofacies show clear lateral zonation and vertical differentiation, with various lithofacies stacking vertically.

The Wufeng–Longmaxi Formation is the main target for shale gas exploration and development in the Sichuan Basin. It conformably overlies the Ordovician Baota Formation limestone and is conformably overlain by the Silurian Hanjiadian/Shiniulan Formation (He et al., 2022; Sun, 2023). Based on well log responses, lithology, and depositional cycles, the Longmaxi shale can be divided into two submembers (Liu et al., 2025b). Based on the development patterns of conodonts, the Longmaxi Formation can be divided into nine distinct conodont zones (LM1–LM9), while the Wufeng Formation is divided into four conodont zones (WF1–WF4). The lower submember (Long-1) is dominated by black shale, grading upward into silty/sandy shale; this lower interval is the primary exploration and development target,

characterized by high organic content and gas content, diverse lithofacies types, and complex vertical variation and stacking relationships.

## 3 Lithofacies classification and types

Shale lithofacies can be classified using various schemes depending on research needs. Factors such as mineral composition and content, organic matter, bedding (lamination) development, paleontology, texture, grain size, and depositional features can all be considered for lithofacies division. In practice, selecting a classification scheme that highlights relevant rock characteristics is fundamental to the study.

### 3.1 Sample selection and preparation

The shale samples used in this study were all sourced from the drill cores of Well A in the southern Sichuan Basin, specifically from the Silurian Wufeng–Longmaxi Formation. To analyze the fracture propagation modes of different lithofacies, targeted sampling was conducted based on the core's lithological characteristics. The samples were primarily used for uniaxial and triaxial compression experiments. Cylindrical specimens were drilled from the cores using a core sampler to dimensions of 2.5 cm × 7.5 cm. Specimens without visible fractures were then cut to 2.5 cm × 5 cm and both ends were polished to ensure flatness.

### 3.2 Experimental methods

Uniaxial and triaxial compression tests were conducted using the RTR-1000 Rock Triaxial Testing System manufactured by Geotechnical Consulting and Testing Systems (GCTS), USA. The rock core specimens were encapsulated with polyolefin heat-shrink tubing and copper end caps. For samples with well-developed bedding, the bedding planes were oriented parallel to the loading direction (0°) during testing.

After placing the specimen in the pressure vessel, hydraulic oil was introduced as the pressure transmission medium. During the triaxial compression tests, the confining pressure was gradually increased at a rate of 0.05 MPa/s until reaching 50 MPa, and then maintained for 30 min to ensure stress equilibrium. Subsequently, axial displacement was applied at a constant rate of 0.001 mm/s using closed-loop servo control, while maintaining a constant confining pressure (Wang R. et al., 2024; Liu et al., 2024). Axial stress, radial strain, and volumetric strain were recorded by sensors. The stress application was terminated when the axial strain reached 8%. All experimental procedures adhered to ASTM D7012-14 standards.

### 3.3 Lithofacies classification scheme

Drawing on previous principles for shale petrofacies classification, this study established a “mineral composition + bedding” lithofacies scheme based on whole-rock mineral

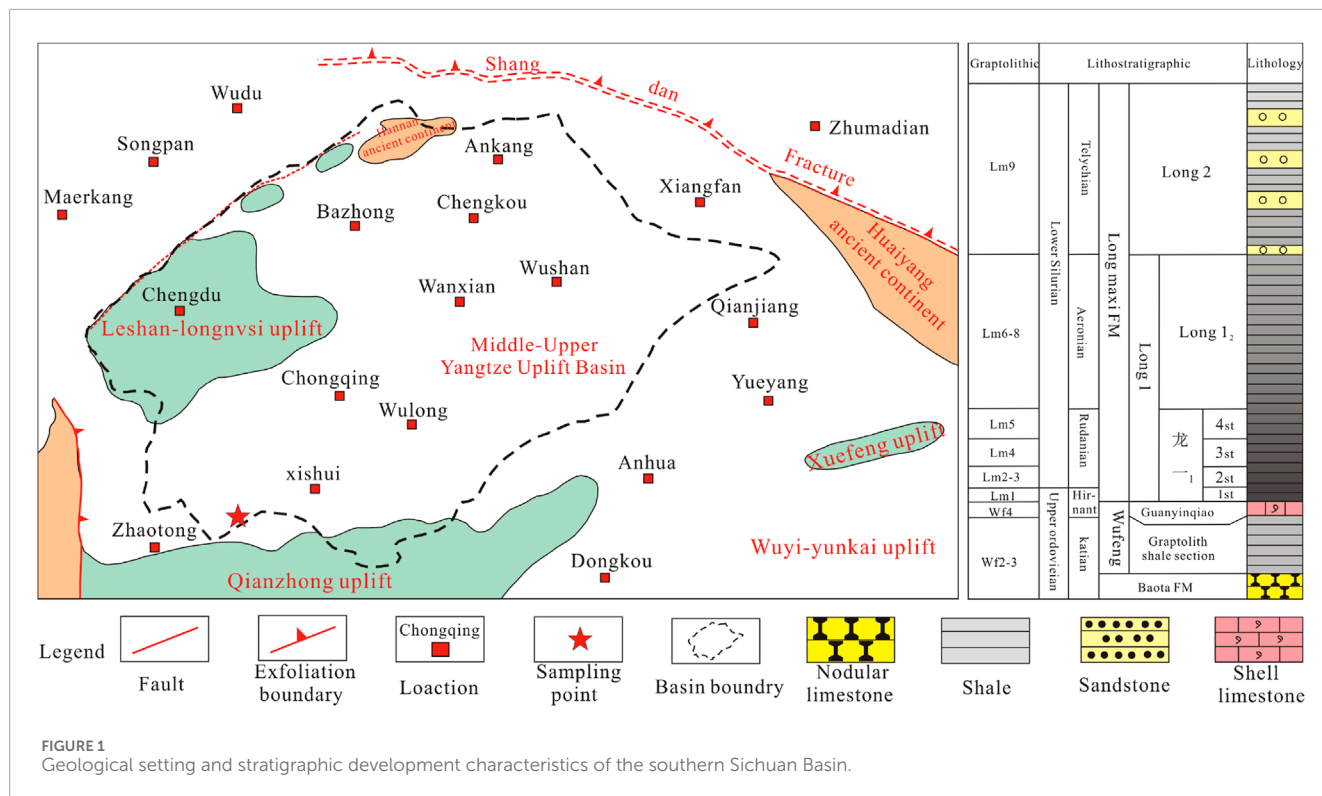


FIGURE 1 Geological setting and stratigraphic development characteristics of the southern Sichuan Basin.

TABLE 1 Shale lithofacies types, minerals and shale development characteristics.

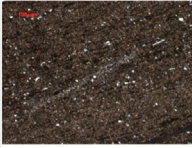
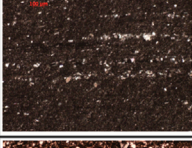
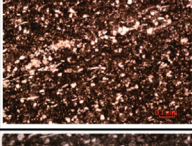
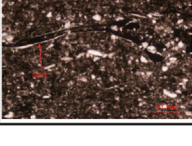
Lithofacies	Mineral characteristics			Structural type
	Siliceous minerals (%)	Clay minerals (%)	Calcareous minerals (%)	
Laminated siliceous shale	50~75	<50	<50	Well-developed bedding, laminated structure
Massive siliceous shale				Poorly developed bedding, massive structure
Laminated clay-rich siliceous shale	25~50	25~50	<37.5	Well-developed bedding, laminated structure
Massive clay-rich siliceous shale				Poorly developed bedding, massive structure
Massive calcareous-siliceous shale	25~50	<37.5	25~50	Poorly developed bedding, massive structure

composition analysis (Shen et al., 2024; Mu et al., 2024; Xue et al., 2024). First, the shale is divided into three broad categories by inorganic mineral content: siliceous shale, calcareous-siliceous mixed shale, and clay-rich siliceous mixed shale. Within each category, lithofacies are further distinguished by the degree of bedding development into laminated and massive types. Using data from a type well on bedding and mineral composition, five lithofacies were identified (Table 1): (i) laminated siliceous shale, (ii) massive siliceous shale, (iii) laminated clay-rich siliceous shale, (iv) massive clay-rich siliceous shale, and (v) massive calcareous-siliceous shale.

### 3.4 Characteristics of different lithofacies

Different lithofacies have distinct mineral compositions and natural fracture (bedding plane) development, which strongly control reservoir fracturing behavior (Yang et al., 2022; Liu et al., 2022a; Cheng et al., 2024). The key characteristics of each identified lithofacies are as follows (Figure 2):

Laminated siliceous shale: Typically developed at the bottom of the Longmaxi Formation. Bedding (lamination) is extremely well-developed, causing the core to break into thin sheets along bedding. Structural (tectonic) fractures are relatively common. Siliceous

Lithofacies	Core	Rock slice	Mineral species	Brittleness	Feature
Layered siliceous shale phase			QZ: 58.4 ARKS: 7.2 Cal: 6.8 Cl: 27.6	$\frac{51.4 \sim 73.2}{58.7}$	Sheet, foliation, natural cracks, biological fossil development
Blocky siliceous shale phase			QZ: 55.9 ARKS: 5.8 Cal: 8.3 Cl: 30	$\frac{55.6 \sim 78.4}{61.2}$	Thick layer block, little foliation development, natural cracks developed
Laminated clay-siliceous mix shale			QZ: 44.8 ARKS: 2.6 Cal: 12.2 Cl: 41.4	$\frac{42.8 \sim 61.6}{46.42}$	Sheet, foliation, natural fracture development, biological fossil less
Blocky-clay siliceous mix shale			QZ: 38.8 ARKS: 4.2 Cal: 16.4 Cl: 40.8	$\frac{44.3 \sim 59.7}{49.4}$	Thick layer block, foliation developed, less Fracture
Blocky-Calcareous siliceous mixed shale			QZ: 41.4 ARKS: 6.6 Cal: 35.6 Cl: 26.4	$\frac{37.58 \sim 48.8}{42.8}$	Thick layer block, fracture development, less foliation

Note: QZ: Quartz; ARKS: Feldspar; Cal: Calcareous minerals; Cl: Clay minerals

FIGURE 2  
Typical core characteristics of the different shale lithofacies types.

mineral content exceeds 50%. Under the microscope, abundant siliceous radiolarians are observed, and the silica often appears as irregularly shaped crystals (indicative of biogenic origin). This facies usually has high organic matter content and is overall black in color.

**Massive siliceous shale:** Concentrated in the upper part of the Longmaxi Formation. It has a high siliceous mineral content, with very few bedding planes observed in core (the rock is thick-bedded and massive). Under the microscope, siliceous mineral grains have regular shapes, indicating they were primarily deposited from distal transport (rather than *in-situ* biogenic silica). This facies typically has lower organic content than the laminated siliceous facies.

**Laminated clay-rich siliceous shale:** Distributed in the middle of the Longmaxi Formation. Bedding and tectonic fractures are moderately developed. Silica content is lower than in the siliceous facies, due to higher clay mineral content. Cores are usually dark gray-black. Under the microscope, distinct clay-rich laminae or streaks are visible. This facies is usually rich in organic matter.

**Massive clay-rich siliceous shale:** Found in both the bottom of the Wufeng Formation and the upper part of the Longmaxi Formation. Cores appear blocky with little bedding development. In the basal Wufeng portion, anomalously high-pressure fractures are observed in core (indicating overpressure was present). This facies has a higher clay content which imparts greater ductility.

**Massive calcareous-siliceous shale:** Mainly present at the top of the Wufeng Formation. It contains significant calcareous components such as fossil shells (bioclasts). It often occurs in thin layers within the sequence and lacks internal lamination. Bedding planes are not developed in this facies.

## 4 Differences in rock mechanical properties

Mechanical properties are a critical factor in shale reservoir stimulation, as they determine the difficulty of fracturing and strongly influence the geometry of the induced fracture network within a layer (Li et al., 2021; Yang et al., 2023b). Brittleness is usually the most important factor considered during hydraulic fracturing design: under stress, a highly brittle rock is more prone to form extensive fractures (Ren et al., 2023). Additionally, the stress-strain behavior of the rock directly affects how fractures propagate.

### 4.1 Brittleness of different lithofacies

Owing to differences in mineral composition, each lithofacies exhibits distinct brittleness. There are various methods to quantify

TABLE 2 Elastic parameters of different minerals in shale.

Mineral type	Elastic modulus (Mpa)	Poisson's ratio	Brittleness coefficient (%)	Normalized brittleness coefficient
Quartz	94.6	0.17	566.47	0.30
Feldspar	69.0	0.28	246.43	0.12
Calcite	68.8	0.31	221.94	0.10
Dolomite	121.00	0.24	431.52	0.11
Pyrite	286.8	0.16	1792.50	1.00
Clay minerals	24.1	0.34	70.88	0.02
Organic matter	6.20	0.14	43.97	0.00

rock brittleness. Two widely used approaches in shale studies are based on (a) mineral composition and (b) rock mechanical parameters. The mineral-composition method defines brittleness as the proportion of “brittle” minerals, but the selection of which minerals are considered brittle can be subjective. The mechanical-parameter method (using elastic modulus and Poisson's ratio, for example,) does not account for the rock's mineralogical makeup, and results can be influenced by specific experimental conditions (e.g., confining pressure, temperature). To overcome these limitations, our study combined both approaches by first evaluating brittleness from mechanical parameters and then incorporating the contributions of different diagenetic minerals (Li, 2022; Liu et al., 2023; 2024). In this study, we first calculated the brittleness coefficient of each individual mineral by combining the brittleness indices of various diagenetic minerals with the mechanical-parameter-derived brittleness. We then normalized these coefficients and, employing the Voigt–Reuss–Hill averaging theory, used the normalized mineral-specific brittleness indices together with their volume fractions to compute the upper threshold, lower threshold, and average brittleness indices of the shale reservoir. Finally, by incorporating the volume fractions of the different diagenetic minerals, we established a composite brittleness index (Bi) for comprehensive brittleness evaluation.

Using this normalized brittleness index, we evaluated the brittleness of each lithofacies. The siliceous shale facies (high quartz content) has a high elastic modulus and low Poisson's ratio, yielding a higher brittleness. The laminated siliceous shale has Bi ranging from ~51.4% to 73.2%, with an average of 58.7%. The massive siliceous shale has Bi between ~55.6% and 78.4%, averaging 61.2%. In the calcareous–siliceous shale facies, the presence of carbonates slightly reduces brittleness: Bi ranges ~46.8%–68.4%, average 51.8%. The clay-rich siliceous shale facies has much higher clay content, which lowers the elastic modulus and increases the rock's toughness (ductility). Accordingly, this facies has the lowest brittleness of the five: Bi ~37.5%–48.4%, average 42.8% (Table 2).

When calculating the brittleness index based on the content of brittle minerals, the normalized brittleness index closely aligns with the quartz content in laminated siliceous shale facies and mixed shale facies. However, in massive siliceous shale facies and their mixed shale counterparts, the normalized brittleness index exhibits

a significant discrepancy compared to the total content of brittle minerals such as quartz and feldspar. These differences in brittleness, along with the vertical distribution of the facies, lead to different modes of stress “unloading” in each lithofacies under stress. In turn, the fracture modes differ, and the resulting fracture vertical distribution, density, and geometry vary from facies to facies.

## 4.2 Stress–strain and energy evolution characteristics

Due to differences in mineralogy and mechanical properties, each lithofacies exhibits distinct behavior in terms of stress concentration and release, stress–strain curve shape, and energy absorption/release during deformation (Xuan and Li, 2023; Yu et al., 2024a). Uniaxial and triaxial compression tests were conducted for the five lithofacies, and the differences in their stress–strain curves and energy evolution are evident.

Under uniaxial compression, all lithofacies show a qualitatively similar stress–strain curve shape characterized by an initial linear elastic stage followed by a rapid drop at failure (Yang et al., 2023a; Wang B. et al., 2023). However, the duration of the elastic stage varies: for example, the laminated clay-rich siliceous shale has a noticeably shorter elastic stage compared to the others. The laminated siliceous shale under uniaxial loading exhibits a relatively long elastic deformation stage, indicating that most of the applied energy is stored elastically with minimal plastic deformation; once it reaches the strength limit, it transitions abruptly into failure (Liu et al., 2025a). Under triaxial compression (with confining pressure), all lithofacies display a clear plastic deformation stage after the elastic stage, before final failure. The nature of this plastic stage and the stress drop at failure differ by lithofacies. The siliceous shale facies (both laminated and massive) under triaxial conditions still maintain a long elastic stage and only a short plastic stage; when failure occurs, the stress drops very abruptly (a sharp “cliff-like” drop). In contrast, the laminated clay-rich siliceous shale shows a shorter elastic stage and a prolonged plastic deformation stage under triaxial loading, and when it fails the stress declines more gradually. Overall, the higher the silica content (brittleness), the longer the elastic deformation phase and

the more sudden the stress drop at failure. The addition of confining pressure increases the rock's yield strength, reduces its brittleness, and enhances ductile behavior in all facies.

During compression, the external work (input energy) is partly stored as elastic strain energy in the rock and partly dissipated (for example, as heat or creating new surfaces) (He et al., 2022). The partitioning of energy into stored elastic energy versus dissipated energy corresponds to different stages of the deformation and cracking process. Based on the stress–strain curve and the energy accumulation/release behavior, the deformation process can be divided into three stages: an elastic stage, a plastic deformation stage, and a failure stage (Schuster et al., 2024). Each stage shows distinct energy accumulation and release characteristics, which vary by lithofacies. Using representative stress–strain–energy curves for each lithofacies (Figure 3), we observe the following: In the elastic stage, the stress–strain curve is linear. Nearly all the input energy is stored as elastic energy in the rock, with minimal energy dissipation. The elastic energy curve rises almost linearly and overlaps the total energy curve (nearly no energy loss). In the plastic deformation stage, the stored elastic energy continues to increase but at a decreasing rate (the elastic energy curve's slope diminishes), while the dissipated energy begins to rise. In this stage, micro-cracks start to nucleate within the rock. As stress input continues and the rock approaches its strength limit, these micro-cracks grow and coalesce. Upon reaching the failure stage, the rock loses stability and fractures. At this point, most of the newly input energy goes into creating fracture surfaces, and the elastic energy that was stored during the earlier stages is suddenly released. The elastic energy curve may actually drop (negative slope) as stored energy is released, and the dissipated energy curve shows a sharp increase due to the energy consumed in generating new fracture surfaces (Zheng et al., 2022).

Comparing energy evolution among lithofacies, the siliceous shale facies (both laminated and massive) have a longer elastic deformation stage and correspondingly accumulate more elastic energy before failure (Yang et al., 2025). Under triaxial conditions, they still store significant elastic energy before a rapid release at failure (indicated by a large stress drop, or “stress drop” magnitude). The clay-rich siliceous shale, on the other hand, transitions to plastic deformation sooner (shorter elastic stage) and exhibits a longer period of plastic deformation. When it fails, the release of energy is more prolonged and a greater proportion of energy is dissipated in driving plastic deformation and crack growth rather than being released suddenly. The calcareous–siliceous shale shows intermediate behavior between the purely siliceous and clay-rich end members.

## 5 Engineering fracturing response of different lithofacies

During shale gas development, horizontal well targets are typically chosen in intervals that are both “brittle and rich” – specifically, layers with high brittleness, high organic content, and high gas content–to maximize the chances of achieving high production. Different shale lithofacies exhibit markedly different responses to hydraulic fracturing, mainly reflected in the ease of fracture initiation and the complexity of the induced fracture network.

### 5.1 Fracturing differences among lithofacies

The failure modes of different lithofacies under stress were examined through laboratory compression tests. By comparing the fracture patterns of samples under uniaxial and triaxial compression, we can infer their fracturing behavior. Under uniaxial compression (no confining pressure), all lithofacies samples failed primarily by the development of vertical tensile splitting fractures (Figure 4). Among these, the siliceous shale facies produced straighter and more penetrating vertical splits, and they were more extensively fractured, which corresponds to field observations where siliceous shale outcrops often exhibit “straight and steep” fractures and faults (Cao et al., 2022; Yan et al., 2024). The laminated siliceous shale in particular showed a high degree of splitting fracture development, reflecting its greater brittleness and tendency to form through-going fractures under stress. This implies that thin siliceous layers can have a higher density of natural faults and fractures. Our experimental observations are consistent with and help validate several key hypotheses from recent studies on shale fracture mechanics. For example, Zhang et al. (2023) demonstrated that fractures in laminated brittle shale tend to follow bedding planes and develop into complex networks with high connectivity. This aligns with our finding that laminated siliceous shale develops high-density, multi-directional fractures under stress. Similarly, Zhang et al. (2022) emphasized that mineralogical brittleness (e.g., quartz-rich facies) correlates with increased fracture complexity and non-uniform fracture widths—features that we also observed in both uniaxial and triaxial tests. These consistencies not only support existing fracture propagation models in heterogeneous media but also extend them by providing empirical evidence of how tectonic–diagenetic history influences lithofacies mechanical properties and thereby controls fracture geometry.

Under triaxial compression (with confining pressure), all lithofacies samples predominantly experienced shear failure (Liu et al., 2024a). However, compared to the uniaxial case, the appearance (orientation and shape) and extent of the fractures differed significantly. In the siliceous shale (laminated and massive) and the calcareous–siliceous shale facies, the fracture angle in the core samples was lower than in the uniaxial case, and failure was characterized by the development of high-angle to vertical splitting fractures along with additional low-angle or horizontal fractures that connected these high-angle fractures. The result was a more complex fracture network within the sample, and individual fracture paths became more tortuous. In contrast, the clay-rich siliceous shale facies showed the most pronounced change in fracture angle: the primary fractures under confinement became much flatter (lower angle) compared to the uniaxial case. Moreover, the overall degree of fracturing in the clay-rich facies was reduced—the fractures were fewer and more planar, and the cylindrical sample remained relatively intact (with much of its original shape preserved).

Comparing the fracturing behavior under reservoir-like confining pressure conditions: all five lithofacies release stored strain energy mainly through shear fracture formation when confined. However, the siliceous shale facies demonstrate a much stronger capacity for fracture generation. Under the same stress conditions, the siliceous facies tend to form shear fractures with higher vertical

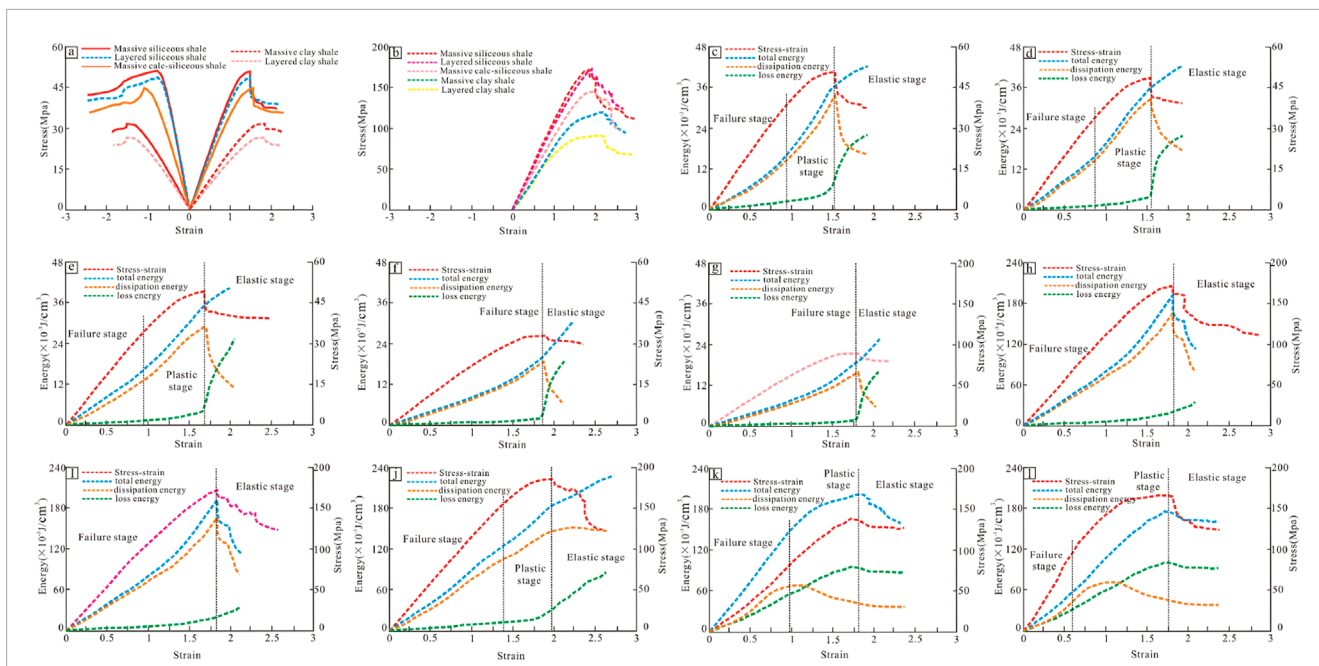


**FIGURE 3** Representative stress–strain–energy curves for different lithofacies under uniaxial and triaxial compression. **(a)** Uniaxial compression stress–strain curve of the samples; **(b)** Triaxial compression stress–strain curve of the samples; **(c)** Strain–energy relationship curve of uniaxial compression for laminated siliceous shale; **(d)** Strain–energy relationship curve of uniaxial compression for massive siliceous shale; **(e)** Strain–energy relationship curve of uniaxial compression for massive calcareous–siliceous mixed shale; **(f)** Strain–energy relationship curve of uniaxial compression for massive clay shale; **(g)** Strain–energy relationship curve of uniaxial compression for layered clay shale; **(h)** Strain–energy relationship curve of uniaxial compression for massive clay shale; **(i)** Strain–energy relationship curve of uniaxial compression for massive calcareous–siliceous mixed shale; **(k)** Strain–energy relationship curve of uniaxial compression for massive siliceous shale; **(l)** Strain–energy relationship curve of uniaxial compression for laminated siliceous shale.

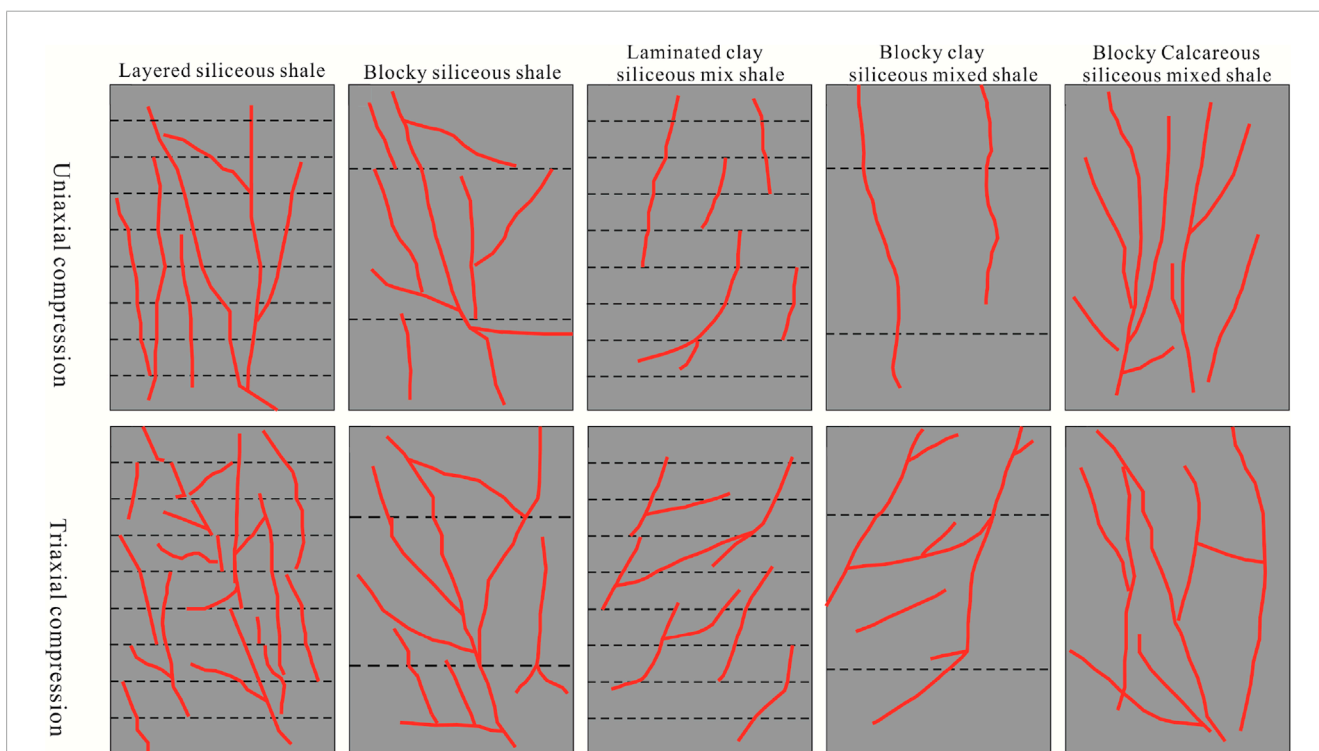


**FIGURE 4** Failure modes of different lithofacies samples under uniaxial (tensile splitting) and triaxial (shear) compression tests.

penetration and longer extension, resulting in a greater number of fractures and a more complex fracture network geometry. This indicates that under *in-situ* conditions, siliceous-rich layers are likely to fracture more extensively and create more complex networks than clay-rich layers.

Overall, fractures developed more extensively under triaxial compression conditions; however, their height was smaller compared to those under uniaxial compression. In laminated siliceous shale, fractures under triaxial compression exhibited a rapid increase in density, with smaller scales and the development of numerous fine, short fractures around the main fractures. These fractures predominantly terminated at bedding planes. In clayey siliceous shale, the fracture propagation orientation also changed notably, with fractures in the core exhibiting smaller dip angles. In this study, we analyzed the post-compression core samples by quantifying fracture density and propagation length. Under uniaxial compression, fractures extended more longitudinally: both laminated siliceous shale and massive siliceous shale developed clear through-going fractures with maximum lengths exceeding 9 cm, corresponding to an equivalent fracture surface density of 4.8–14.6 m<sup>-2</sup>. By contrast, under triaxial compression only a few specimens formed connected through-going fractures, and these were generally shorter than 6 cm. Furthermore, fracture density under triaxial conditions varied markedly, with laminated siliceous shale reaching an equivalent maximum fracture density of 38 m<sup>-2</sup>.

Comparative analysis suggests that under triaxial compression, the lateral deformation of the rock is constrained by confining pressure, leading to a shift in stress release from large-scale shear failure to “planar” stress release. This results in densely developed but short fractures. Under both uniaxial and triaxial compression conditions, laminated siliceous shale exhibited the highest fracture propagation capacity.

Previous studies have shown that shale brittleness correlates with the morphology and width distribution of induced fractures (Shi and Lin, 2021). Under the same confining pressure, as the brittleness index increases, hydraulic fracture patterns transition from simple straight fractures to complex network fractures. Additionally, high-brittleness shales tend to develop fractures with non-uniform widths, whereas low-brittleness shales more often have fractures with relatively uniform width (Yang et al., 2021). In highly ductile layers, stress is relieved in a more linear, penetrative fashion, resulting in a single, simple fracture. In contrast, in highly brittle layers, stress is relieved by “planar extension,” meaning the stress-unloading region expands along multiple planes, producing a greater number of fractures with more complex (Figure 5).

## 5.2 Stress response mechanism of lithofacies stacking combinations

During deposition of the Wufeng–Longmaxi shale, frequent changes in sediment supply and water conditions led to vertical lithofacies heterogeneity, with multiple lithofacies stacked in sequence. In the subsurface, the thickness of an individual lithofacies layer is generally less than 10 m (often <5 m for the thin-bedded facies in the study area). The contacts between different lithofacies, as well as bedding planes within them, serve as natural mechanical

discontinuities and weak surfaces. When stress propagates across these weak interfaces, the fracturing response can vary greatly.

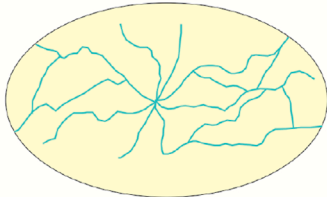
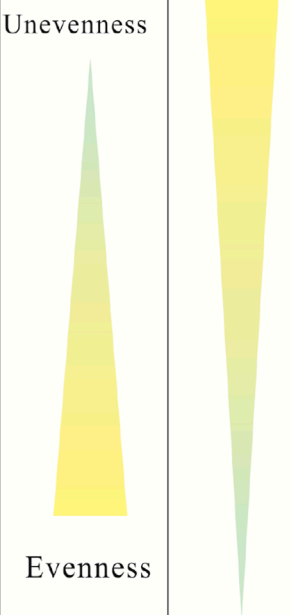
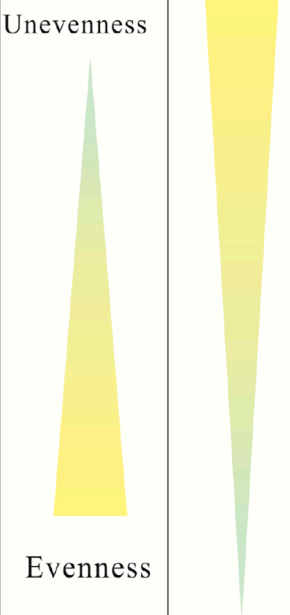
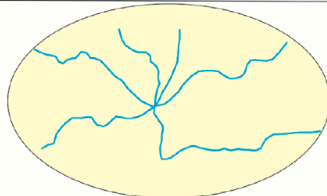
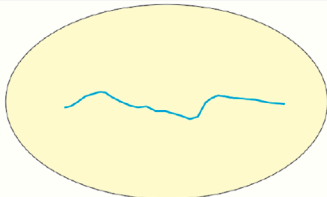
Rocks on either side of a lithofacies contact or bedding plane often have different mechanical parameters such as shear strength, elastic modulus, and Poisson's ratio (Yang et al., 2021; Liu et al., 2022b). Based on mechanical property contrasts, we can conceptually classify certain lithofacies layers as relatively “strong barriers” and others as “weak barriers.” When a propagating fracture (stress) moves from a strong, stiff layer into a weaker layer, the stronger layer acts as a barrier that can impede fracture growth. This stress barrier effect can lead to several outcomes at the interface: the fracture may penetrate through the interface, arrest (stop) at the interface, generate multiple branch fractures, open up the interface (delamination), or twist/turn along the interface. Conversely, when stress propagates from a weak layer into a stronger layer, the weak layer tends to absorb and dissipate some of the stress (“stress absorption” effect), which limits the height growth of fractures (Wang et al., 2021) and can even cause the fracture to terminate at the contact.

Considering the vertical distribution of lithofacies in the study area, three typical lithofacies stacking combinations can be identified, as illustrated in Figure 6. Each combination exhibits a distinct stress response mechanism during fracturing:

Laminated siliceous shale overlaid by laminated clay-rich siliceous shale: These thinly layered facies commonly occur at the bottom of the Longmaxi Formation. They feature well-developed bedding and a certain amount of natural fractures. The contacts and laminations act as pronounced stress barriers. As stress propagates upward through these layers, the strong siliceous layer (high elastic modulus) can be considered a “strong barrier layer” and the overlying clay-rich siliceous layer a relatively “weak barrier layer.” When the fracture-driving stress passes from the siliceous into the clay-rich layer, the drop in elastic modulus causes a local change in stress direction at the interface. The fracture propagation direction changes, and in the clay-rich layer the fracture loses some of its straightness. A single fracture may develop in a stepped, stair-case fashion through successive layers, and at some bedding interfaces the fracture may even bifurcate (split) into branches. The result is a vertically stepping fracture with branch fractures at some layer boundaries (Figure 6A).

Massive clay-rich siliceous shale beneath massive calcareous–siliceous shale: In this combination, often found in the middle of the sequence (e.g., upper Longmaxi and lower Wufeng), the fracture propagation is relatively simple. The layer thicknesses are larger and overall brittleness is lower (due to more clay and carbonate). When fracturing, shear cracks can propagate a relatively long distance in the stronger calcareous–siliceous layer, forming a dominant vertical tensile fracture. Some fractures may even cross into adjacent layers (cross-layer propagation). However, when the stress reaches the clay-rich siliceous layer, which has a lower elastic modulus and may have some bedding, the fracture tends to deflect or even terminate at the bedding plane. The vertical extension of the fracture is thus limited in the clay-rich layer (Figure 6B). Overall, fracturing in this combination produces mostly planar, penetrating fractures with limited branching, and the fractures may not propagate far into the weaker clay-rich layer.

Massive siliceous shale adjacent to massive clay-rich siliceous shale: In this scenario (commonly the uppermost part of the sequence in the study area), the siliceous shale has very few bedding planes and high strength, so fracturing within it is dominated

Brittleness index	Fracture propagation pattern		Fracture width	Density
>50	map cracking, strong penetration and plane communication ability			
30~50	Multi-slit, multiple extension directions, increased complexity			
<30	simple fracture morphology, single extension direction. line type fracture			

**FIGURE 5** Schematically illustrates the relationship between shale brittleness and the characteristics of the induced fracture network.

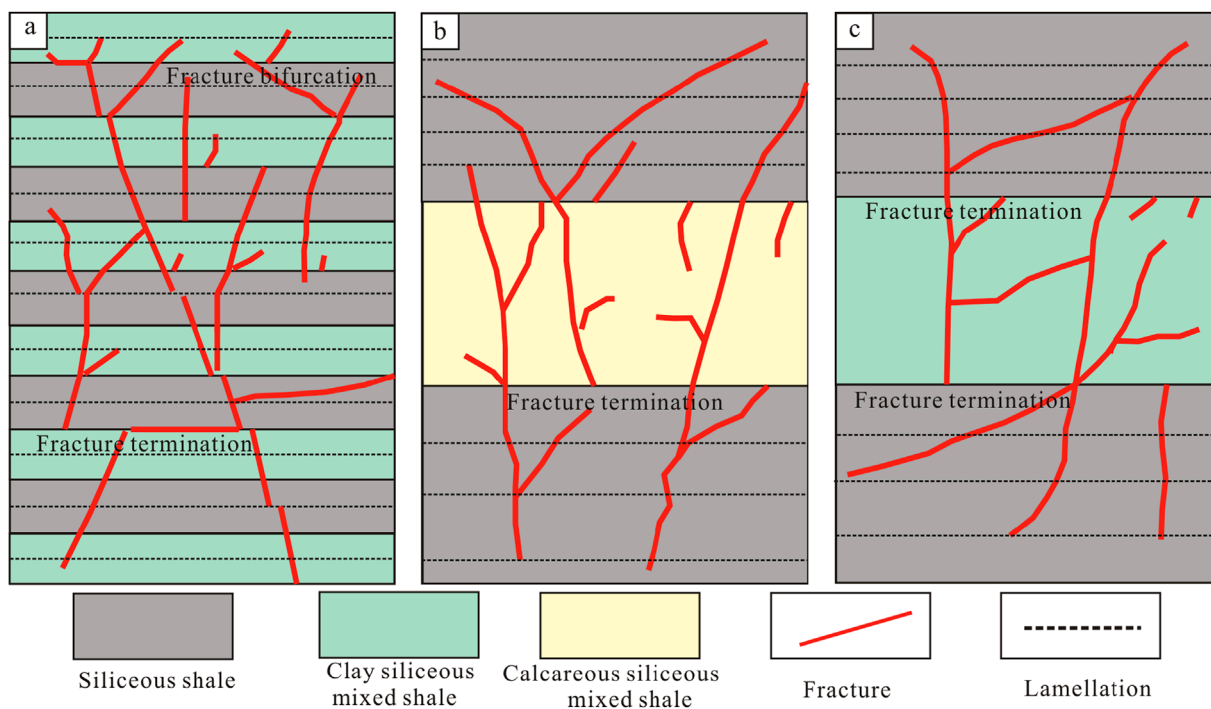


**FIGURE 6** Schematic of fracture propagation behavior in different lithofacies stacking combinations. (a) laminated siliceous shale with laminated clay-rich siliceous shale; (b) massive clay-rich siliceous shale with massive calcareous-siliceous shale; (c) massive siliceous shale with massive clay-rich siliceous shale.

by tensile splitting. The stress is largely released via shear failure, resulting in a high density of fractures, with notable branching and strong lateral connectivity within the siliceous layer. However, when these fractures propagate into the massive clay-rich shale, the mode of stress release changes. A portion of the stress is consumed by plastic deformation of the clay minerals, which acts to absorb energy. Consequently, fracture propagation in the clay-rich layer is restricted, and fractures often terminate as the available energy is dissipated (Figure 6C). The fractures that do enter the clay-rich layer may become blunted or stop, preventing further vertical growth.

## 6 Implications for hydraulic fracturing operations

Successful shale gas production relies on volumetric fracturing of organic-rich shale to create a complex fracture network that connects isolated pores and increases reservoir permeability. Reservoir stimulation designs aim to maximize the complexity of the fracture system to contact as much high-quality reservoir rock as possible (Su et al., 2015; Ferguson et al., 2021). Given that sedimentary and diagenetic processes cause the vertical stacking of multiple shale lithofacies with differing mechanical properties and natural fracturing, hydraulic fracturing behavior (fracture geometry and propagation) will vary throughout the sequence. Based on the vertical lithofacies combinations in the study area and their stress response characteristics, the following implications can be drawn for fracturing design and execution:

**Bottom interval (thin laminated siliceous shale + laminated clay-rich shale combination):** This interval, often the most organic-rich, has well-developed bedding and natural fractures. During hydraulic fracturing, these pre-existing fractures can influence the propagation of new fractures on a local scale. Fracturing this interval is likely to activate the natural fractures, which provides some pressure relief and diversion. Meanwhile, bedding planes and lithofacies contacts cause the fracture paths to deflect, resulting in irregular fractures within each thin layer and forming a three-dimensional mesh-like fracture network (Cheng et al., 2022; Hu et al., 2024). This dense network of small interconnected fractures can effectively connect a broad volume of the reservoir in the horizontal plane. Operational recommendation: Use slickwater (low-viscosity, friction-reduced fluid) and perform multiple, closely spaced fracturing stages to promote the creation of numerous fractures. The low viscosity fluid can slip through thin natural fractures and generate complex new fractures. Repeating injections in the same interval (re-fracturing stages) can help activate more fractures. This strategy will enhance the complexity and density of the fracture network and improve stimulation effectiveness in this interval.

**Middle interval (massive clay-rich siliceous shale + massive calcareous-siliceous shale combination):** In this combination, the overall formation brittleness is reduced and bedding is less developed, while individual layer thickness is greater. The higher clay content increases the ductility of the formation, meaning much of the fracturing energy can be absorbed (the “stress absorption” effect) rather than creating fractures. Under the same treatment conditions, this interval’s fracturing ability is weaker, tending to form fewer

fractures, though individual fractures may be larger. The lateral (planar) connectivity of fractures is lower, and due to the increased plasticity, the fractures that do form are more prone to closure under *in-situ* stress after pumping stops. Operational recommendation: Use a higher pump rate and higher proppant concentration during fracturing. A higher fluid injection rate delivers more energy to drive fractures farther and counteracts the energy absorption by the formation, while a greater volume of proppant helps prop fractures open against the formation’s tendency to creep and close. This will enhance the stress penetration capability, increase fracture height penetration and lateral connectivity, and mitigate fracture closure in this less brittle interval.

**Top interval (massive siliceous shale + massive clay-rich siliceous shale combination):** Here, individual layers are thick and bedding is relatively absent. In the siliceous layer, the lack of bedding “barriers” means stress can propagate freely, resulting in larger vertical fracture height growth. However, this strong vertical penetration tends to produce a lower density of fractures in the horizontal plane (i.e., fewer fracture branches). As a result, the fracture network may have limited areal extent. Operational recommendation: Use smaller fluid volumes per stage but increase the number of stages (i.e., use small job sizes with more frequent fracturing) and deploy temporary plugging agents during treatment. The temporary plugging agents (diverters) can be injected to temporarily block dominant fractures and force the fluid to initiate new fractures in other directions. This helps alter the fracture propagation direction within the layer and encourages the formation of a more complex fracture network. By increasing the number of fractures and their distribution, the lateral coverage of the fractures is expanded. Such an approach can compensate for the natural tendency of this interval to form simpler, planar fractures, ultimately achieving a better stimulation result.

This research has several strengths. It provides a systematic linkage between geological history (tectonic stress and diagenetic alteration) and shale fracturing behavior, supported by controlled laboratory experiments. The comprehensive mechanical and fracturing data across multiple lithofacies give a robust understanding of how rock heterogeneity shapes fracture networks. These contributions deepen theoretical understanding and offer practical guidance for field stimulation strategies. However, some limitations should be noted. Our experiments are conducted on core samples under idealized conditions, which may not capture all complexities of *in-situ* reservoir environments (such as natural fluid interactions, scale effects, and heterogeneity beyond our sampling). The study focuses on a specific shale formation in the Sichuan Basin, and while many findings are broadly applicable, local geological variations could influence fracturing outcomes elsewhere. Future work should include validation with field-scale data and numerical modeling to account for larger-scale heterogeneity and more complex stress states.

## 7 Conclusion

- (1) In the Long-1 submember of the Wufeng–Longmaxi shale (southern Sichuan Basin), five shale lithofacies are developed: laminated siliceous shale, massive siliceous shale, laminated clay-rich siliceous shale, massive clay-rich siliceous

shale, and massive calcareous–siliceous shale. Of these, the two siliceous shale facies are the most brittle, the calcareous–siliceous shale facies has intermediate brittleness, and the clay-rich siliceous shale facies are the least brittle.

- (2) Under uniaxial stress, all lithofacies samples primarily develop vertical tensile (splitting) fractures. Under confining pressure conditions, the siliceous shale facies, due to a larger stress drop and a higher elastic energy release ratio, exhibit the most extensive failure, unloading stress by “planar extension” of fractures. In these high-brittleness layers, fractures in the stress-unloading zone propagate in a planar fashion. The laminated calcareous–siliceous shale facies has the second strongest fracture propagation capacity, while the laminated clay-rich siliceous shale facies shows the weakest ability to generate fractures.
- (3) In a combination of laminated siliceous shale and clay-rich siliceous shale layers, bedding planes create a significant “stress barrier” effect. Vertical hydraulic fractures develop branching in a stepped manner, forming a complex fracture network with short segments but strong interconnectivity. In a combination of thinly layered (laminated) calcareous–siliceous shale and clay-rich siliceous shale, hydraulic fracturing tends to produce mostly through-going fractures with moderate interconnection between fractures. In a combination of massive siliceous shale and massive clay-rich siliceous shale, shear-dominated fracturing prevails with strong vertical stress penetration, but the planar fracturing ability is weak—the resulting fractures have low density and simple geometry. The outcomes of this study provide a reference for optimizing stimulation strategies and operational parameters for shale formations with different lithofacies stacking configurations.
- (4) The present findings offer a broad theoretical framework and practical guidelines for hydraulic fracturing in shale reservoirs globally. By linking lithofacies mechanical properties (shaped by tectonic–diagenetic history) to fracture patterns, the study contributes to global understanding of shale reservoir mechanics. Practically, the results highlight how to target brittle siliceous intervals and tailor fracturing parameters (such as fluid viscosity or proppant volume) to the local lithofacies architecture. Thus, our study offers guidance for designing more effective stimulation programs in marine shale formations worldwide, enhancing recovery while reducing uncertainty.

## References

- Cao, Q., Ye, X., Liu, Y., Wang, P., and Jiang, K. (2022). Effect of different lithological assemblages on shale reservoir properties in the Permian Longtan Formation, southeastern Sichuan Basin: case study of Well X1. *PLOS ONE* 17 (8), e0271024. doi:10.1371/journal.pone.0271024
- Chen, Y. N., Yang, K., Wu, W., Yang, Y., Yang, X., and Ma, K. (2023). Favorable lithofacies and pore characteristics of the Permian Longtan Formation shale in the southern Sichuan Basin. *Energy Geosci.* 4 (3), 100193. doi:10.1016/j.engeos.2023.100193
- Cheng, G., Jiang, B., Li, F., Li, M., and Song, Y. (2022). Distribution prediction of shale deformation structures in tectonically complex area based on relationship between geological structures and shale deformation. *Front. Earth Sci.* 10, 813074. doi:10.3389/feart.2022.813074
- Cheng, S., Sheng, M., and Deng, C. (2024). Identification of different lithofacies laminations in oil shale and their mechanical properties. *Front. Energy Res.* 11, 1321853. doi:10.3389/feart.2023.1321853
- El-Sayed, A. S., Mabrouk, W. M., and Metwally, A. M. (2024). Utilizing post-stack seismic inversion for delineation of gas-bearing sand in a Pleistocene reservoir, Baltim gas field, Nile Delta, Egypt. *Sci. Rep.* 14, 29596. doi:10.1038/s41598-024-78186-9
- Fan, C. H., Li, H., Zhao, S. X., Qin, Q. R., Fan, Y., Wu, J. F., et al. (2020). Formation stages and evolution patterns of structural fractures in marine shale: case study of the Lower Silurian Longmaxi Formation in the Changning area of the southern Sichuan Basin, China. *Energy Fuel* 34 (8), 9524–9539. doi:10.1021/acs.energyfuels.0c01748
- Fan, C. H., Nie, S., Li, H., Radwan, A. E., Pan, Q. C., Shi, X. C., et al. (2024). Quantitative prediction and spatial analysis of structural fractures in deep shale gas

## Data availability statement

The original contributions presented in the study are included in the article/supplementary material, further inquiries can be directed to the corresponding author.

## Author contributions

LY: Validation, Writing – review and editing, Methodology, Writing – original draft. XP: Formal Analysis, Methodology, Writing – review and editing. YH: Investigation, Writing – original draft. AL: Project administration, Writing – original draft.

## Funding

The author(s) declare that no financial support was received for the research and/or publication of this article.

## Conflict of interest

Author YH was employed by Geological Logging Company (Geological Research Institute) of Daqing Oilfield Co., Ltd.

The remaining authors declare that the research was conducted in the absence of any commercial or financial relationships that could be construed as a potential conflict of interest.

## Generative AI statement

The author(s) declare that no Generative AI was used in the creation of this manuscript.

## Publisher's note

All claims expressed in this article are solely those of the authors and do not necessarily represent those of their affiliated organizations, or those of the publisher, the editors and the reviewers. Any product that may be evaluated in this article, or claim that may be made by its manufacturer, is not guaranteed or endorsed by the publisher.

- reservoirs within complex structural zones: a case study of the Longmaxi Formation in the Luzhou area, southern Sichuan Basin, China. *J. Asian Earth Sci.* 263, 106025. doi:10.1016/j.jseas.2024.106025
- Feng, Z. Q., Hao, F., Zhou, S., Wu, W., Tian, J., Xie, C., et al. (2020). Pore characteristics and methane adsorption capacity of different lithofacies of the Wufeng Formation–Longmaxi Formation shales, southern Sichuan Basin. *Energy Fuel* 34 (7), 8046–8062. doi:10.1021/acs.energyfuels.0c00782
- Ferguson, B., Agrawal, V., Sharma, S., Hakala, J. A., and Xiong, W. (2021). Effects of carbonate minerals on shale-hydraulic fracturing fluid interactions in the Marcellus Shale. *Front. Earth Sci.* 9, 695978. doi:10.3389/feart.2021.695978
- He, R., Li, R., Zhu, Z. M., and Sun, X. (2022). Anisotropy characterization of the elasticity and energy flow of Longmaxi shale under uniaxial compression. *Energy Rep.* 8, 1410–1424. doi:10.1016/j.egyr.2021.12.050
- He, S., Tan, W., Li, H., Wang, Y., Niu, P., and Qin, Q. (2025). Mineralogical and lithofacies controls on gas storage mechanisms in organic-rich marine shales. *Energy Fuel* 39 (8), 3846–3858. doi:10.1021/acs.energyfuels.4c05685
- He, X. Y., Zhang, K., Jiang, S., Jiang, Z. X., Wang, X. Y., Jiang, W., et al. (2025). Influencing factors and quantitative prediction of gas content of deep marine shale in Luzhou block. *Sci. Rep.* 15, 1896. doi:10.1038/s41598-025-86095-8
- Hou, M. R., Liang, B., and Sun, W. J. (2023). Influence of mineral interface stiffness on fracture propagation law of shale hydraulic fracturing. *Res. Eval. Dev.* 13 (1), 100–107. doi:10.13809/j.cnki.cn32-1825/te.2023.01.011
- Hu, J., Zhang, L., and He, M. (2024). Investigation of the bedding effect on coal rock under Brazilian splitting tests. *Front. Earth Sci.* 12, 1416035. doi:10.3389/feart.2024.1416035
- Jiang, S., Zhou, Q., Li, Y., Yang, R., Zhao, R., and Ma, D. (2025). Conditions for shale gas accumulation and the gas-bearing factors of the Wufeng-Longmaxi formation in the Laifeng–Xianfeng area. *Sci. Rep.* 15, 314. doi:10.1038/s41598-024-84415-y
- Li, H. (2022). Research progress on evaluation methods and factors influencing shale brittleness: a review. *Energy Rep.* 8, 4344–4358. doi:10.1016/j.egyr.2022.03.120
- Li, H., Duan, H., Qin, Q., Zhao, T., Fan, C., and Luo, J. (2025). Characteristics and distribution of tectonic fracture networks in low permeability conglomerate reservoirs. *Sci. Rep.* 15, 5914. doi:10.1038/s41598-025-90458-6
- Li, H., He, S., Radwand, A. E., Xie, J. T., and Qin, Q. R. (2024). Quantitative analysis of pore complexity in lacustrine organic-rich shale and comparison to marine shale: insights from experimental tests and fractal theory. *Energy Fuel* 38 (17), 16171–16188. doi:10.1021/acs.energyfuels.4c03095
- Li, H. G., Li, H. H., and Xu, G. S. (2021). Influence of water content on mechanical characteristics of weakly cemented sandstone. *J. Min. Strata Control Eng.* 3 (4), 60–66. doi:10.13532/j.jmsce.cn10-1638/td.20210610.003
- Li, Y., He, J. H., Deng, H. C., Li, R. X., Li, Q., Fu, M. Y., et al. (2024). Effect of lithofacies assemblages on multi-scale fractures in the transitional shale and its implications for shale gas exploration. *Geoenergy Sci. Eng.* 233, 212562. doi:10.1016/j.geoen.2023.212562
- Liu, G., Shang, D., Zhao, Y., and Du, X. (2024). Characterization of brittleness index of gas shale and its influence on favorable block exploitation in southwest China. *Front. Earth Sci.* 12, 1389378. doi:10.3389/feart.2024.1389378
- Liu, H., Zhang, S., Liu, Y., Zhang, P., Wei, X., Wang, Y., et al. (2022a). Characteristics of lithofacies combinations and reservoir property of carbonate-rich shale in Dongying Depression, Eastern China. *Front. Earth Sci.* 10, 857729. doi:10.3389/feart.2022.857729
- Liu, H. M., Ni, C. Y., Wang, X. H., Wang, M. Q., Ma, X. Q., Cao, L., et al. (2024a). Particle flow analysis of crack propagation characteristics of cross jointed rock under uniaxial compression. *Chin. J. Rock Mech. Eng.* 43 (S2), 3710–3721. doi:10.13722/j.cnki.jrme.2023.0359
- Liu, J., Wu, J., Xiong, J., Li, B., Liu, X., and Liang, L. (2022b). Rock mechanical properties and energy evolution characteristics of different shale lithofacies in marine-continental transition facies. *Spec. Oil Gas. Res.* 29 (6), 83–90. doi:10.3969/j.issn.1006-6535.2022.06.010
- Liu, J. F., He, X., Xue, F. J., Dai, J. J., Yang, J. X., Huang, H. Y., et al. (2024b). The influence of natural fractures of multi-feature combination on seepage behavior in shale reservoirs. *J. Min. Strata Control Eng.* 6 (1), 131–140. doi:10.13532/j.jmsce.cn10-1638/td.20240018.001
- Liu, Z., Gao, K., Liu, Y., Zhu, C., and Zhang, Y. (2025a). Piezoelectric characteristics of coal rock leakage under uniaxial compression. *Sci. Rep.* 15, 4432. doi:10.1038/s41598-025-88269-w
- Liu, Z., Zhang, J., Sun, Y., Yu, Z., and Ren, R. (2023). A new bayesian-based brittleness prediction method for the pingdiquan formation in the eastern shiqiantan depression of the east jungggar basin. *Front. Earth Sci.* 11, 1163938. doi:10.3389/feart.2023.1163938
- Liu, Z. J., Jiang, Z. X., Wei, F. B., Yuan, T., and Li, F. (2025b). Shale gas accumulation mechanism of deep-buried marine shale of upper ordovician Wufeng Formation to lower silurian Longmaxi Formation in the southeast Sichuan Basin. *Petroleum Res.* 10(1):137–148. doi:10.1016/J.PTLRS.2024.07.006
- Mu, Z., Li, C., Liu, Z., Liu, T., Zhang, K., Mu, H., et al. (2024). A deep learning identification method of tight sandstone lithofacies integrating multilayer perceptron and multivariate time series. *Sci. Rep.* 14, 31252. doi:10.1038/s41598-024-82607-0
- Ren, L., Yu, Z., Zhao, J., Lin, R., Wu, J. F., Song, Y., et al. (2023). Influence of fault attributes of deep shale gas on fracturing fracture network. *Spec. Oil Gas. Res.* 30 (2), 95–100. doi:10.3969/j.issn.1006-6535.2023.02.013
- Schuster, V., Rybacki, E., Bonnelye, A., and Dresen, G. (2024). Deformation behavior and seismic characteristics of sandy facies Opalinus clay during triaxial deformation under dry and wet conditions. *Rock Mech. Rock Eng.* 57, 4787–4813. doi:10.1007/s00603-024-03802-z
- Shen, Y., Wu, S., Wu, K., Xing, H., Wang, C., Li, Y., et al. (2024). Lithofacies evaluation of paleogene yingxiangling shale oil, qaidam basin. *Energy Fuel* 38 (11), 9546–9562. doi:10.1021/acs.energyfuels.3c04668
- Shi, C., and Lin, B. (2021). Principles and influencing factors for shale formations. *Petrol. Sci. Bull.* 6 (1), 92–113. doi:10.3969/j.issn.2096-1693.2021.01.008
- Su, Y., Ren, L., Meng, F., Xu, C., and Wang, W. (2015). Theoretical analysis of the mechanism of fracture network propagation with stimulated reservoir volume (SRV) fracturing in tight oil reservoirs. *PLOS ONE* 10 (5), e0125319. doi:10.1371/journal.pone.0125319
- Sun, H., Cai, X., Hu, D., Lu, Z., Zhao, P., Zheng, A., et al. (2023). Theory, technology and practice of shale gas three-dimensional development: a case study of Fuling shale gas field in Sichuan Basin, SW China. *Petrol. Explor. Dev.* 50 (3), 651–664. doi:10.1016/s1876-3804(23)60417-3
- Sun, Z. (2023). Superimposed hydrocarbon accumulation through multi-source and multi-stage evolution in the Cambrian Xixiangchi Group of eastern Sichuan Basin: a case study of the Pingqiao gas-bearing anticline. *Energy Geosci.* 4 (1), 131–142. doi:10.1016/j.engeos.2022.09.001
- Wang, B., Lu, C., Cui, F., and Zhang, Z. (2023). Uniaxial compression test research on rock creep disturbance characteristics based on CT scanning. *J. Min. Strata Control Eng.* 4 (3), 43–53. doi:10.13532/j.jmsce.cn10-1638/td.2023.03.002
- Wang, R., Liu, Y., Li, Z., Wang, D., Wang, G., Lai, F., et al. (2024). Microscopic pore structure characteristics and controlling factors of marine shale: a case study of Lower Cambrian shales in the Southeastern Guizhou, Upper Yangtze Platform, South China. *Front. Earth Sci.* 12, 1368326. doi:10.3389/feart.2024.1368326
- Wang, R., Wang, G., Zhao, G., Qian, M., Liu, Y., He, W., et al. (2023). Geological characteristics and resources potential of shale oil in chang 7 member of upper triassic yanhang formation in fuxian area, southern ordos basin, western China. *Unconv. Resour.* 3, 237–247. doi:10.1016/j.unres.2023.06.001
- Wang, Y., Hou, B., Wang, D., and Jia, Z. (2021). Features of fracture height propagation in cross-layer fracturing of shale oil reservoirs. *Petrol. Explor. Dev.* 48 (2), 469–479. doi:10.1016/s1876-3804(21)60038-1
- Wang, Y. Y., Liu, H., Hu, X. H., Dai, C., and Fang, S. (2024). Fracture network types revealed by well test curves for shale reservoirs in the Sichuan Basin, China. *Energy Geosci.* 5 (1), 100135. doi:10.1016/j.engeos.2022.09.005
- Wu, Z. W., Cui, C. Z., Jia, P. F., Wang, Z., and Sui, Y. F. (2022). Advances and challenges in hydraulic fracturing of tight reservoirs: a critical review. *Energy Geosci.* 3 (4), 427–435. doi:10.1016/j.engeos.2021.08.002
- Xiong, L., Dong, X., Wang, T., Feng, S., Wei, L., Zhou, H., et al. (2025). Accurate lithofacies identification in deep shale gas reservoirs via an optimized neural network recognition model, Qiongzhusi Formation, southern Sichuan. *Sci. Rep.* 15, 8714. doi:10.1038/s41598-025-86088-7
- Xuan, Z., and Li, H. (2023). Mechanical characteristics and energy evolution of rock with circular hole defects. *PLOS ONE* 18 (12), e0295675. doi:10.1371/journal.pone.0295675
- Xue, Y., Dang, W., Zhang, Q., Liu, J., Shanguan, L., Lei, Y., et al. (2024). Lithofacies and its reservoir characteristics of marine-continental transitional shales: a case study of Shanxi Formation in Eastern Ordos Basin. *Energy Fuel* 38 (19), 18441–18456. doi:10.1021/acs.energyfuels.4c02981
- Yan, W., Wang, C., Yin, S., Wen, Z., Zheng, J., Fu, X., et al. (2024). A log-based method for fine-scale evaluation of lithofacies and its applications to the Gulong shale in the Songliao Basin, Northeast China. *Energy Geosci.* 5 (3), 100291. doi:10.1016/j.engeos.2024.100291
- Yang, G., Zeng, J., Qiao, J., Liu, Y., Liu, S., Jia, W., et al. (2022). Role of organic matter, mineral, and rock fabric in the full-scale pore and fracture network development in the mixed lacustrine source rock system. *Energy Fuel* 36 (15), 8161–8179. doi:10.1021/acs.energyfuels.2c01484
- Yang, L., Li, J., Jiang, C., and Huang, X. (2023a). Analysis of acoustic emission parameters and time-frequency characteristics in the process of rock sample fracture. *J. Min. Strata Control Eng.* 4 (1), 67–77. doi:10.13532/j.jmsce.cn10-1638/td.20220923.003
- Yang, S., Liu, P. Z., and Lu, W. (2023b). Study on triaxial compression tests on briquette coal specimens with different binder contents. *J. Min. Strata Control Eng.* 5 (2), 46–54. doi:10.13532/j.jmsce.cn10-1638/td.2023.02.001
- Yang, Y., Li, X., Ju, Y., Li, G., and Li, X. (2025). Multifactor coupled evaluation model of fracability based on a combinatorial weighting method: a case study of the low-permeability sandstone reservoirs of Yanhang Formation, southwestern Ordos Basin, China. *Rock Mech. Rock Eng.* 58, 905–925. doi:10.1007/s00603-024-04193-x
- Yang, Z. Z., Yu, Q. S., and Li, X. G. (2021). Research progress and prospect of shale deformation and failure characteristics. *Sci. Tech. Eng.* 21 (26), 11015–11022. doi:10.3969/j.issn.1671-1815.2021.26.003

- Yu, W. J., Pan, B., Wu, G. S., and Guo, H. X. (2024a). Experimental study on mechanical characteristics of rock of trapezoidal cross section under the equivalent non-uniform loading conditions. *J. Min. Strata Control Eng.* 6 (3), 108–117. doi:10.13532/j.jmsce.cn10-1638/td.2024.03.001
- Yu, Y., Song, Z., Liu, J., Yang, Y., and Dong, X. (2024b). Energy evolution mechanism of structural surfaces in sandstones with different dips based on the energy principle. *PLOS ONE* 19 (3), e0300931. doi:10.1371/journal.pone.0300931
- Zhang, Y. H., Ma, J. F., Wang, Y., Wang, F., Li, X., and Zhao, L. X. (2022). Quantification of the fracture complexity of shale cores after triaxial fracturing. *Front. Earth Sci.* 10, 863773. doi:10.3389/feart.2022.863773
- Zhang, Z., Zhong, A., Yang, F., Zhang, L., Lu, M., Chai, L., et al. (2023). Experimental study on the hydraulic fracture propagation of laminar argillaceous limestone continental shale. *Front. Earth Sci.* 11, 1193205. doi:10.3389/feart.2023.1193205
- Zhao, K. K., Wang, L., Jiang, P. F., Sun, X. D., Feng, Y. J., and Zheng, Y. F. (2023). Three-dimensional numerical simulation of hydraulic fracture spatial steering. *J. Min. Strata Control Eng.* 5 (3), 32–42. doi:10.13532/j.jmsce.cn10-1638/td.2023.03.004
- Zheng, G., Tang, Y., Zhang, Y., Gao, Y., Zhu, G., Gao, M., et al. (2022). Study on failure difference of hard rock based on a comparison between the conventional triaxial test and true triaxial test. *Front. Earth Sci.* 10, 923611. doi:10.3389/feart.2022.923611
- Zheng, H., Zhang, J., and Qi, Y. (2020). Geology and geomechanics of hydraulic fracturing in the Marcellus shale gas play and their potential applications to the Fuling shale gas development. *Energy Geosci.* 1 (1-2), 36–46. doi:10.1016/j.engeos.2020.05.002
- Zhou, Z. Y. (2023). Mechanism of fracture extension and process countermeasures in grain-type shale oil reservoirs. *Spec. Oil Gas. Res.* 30 (6), 141–149. doi:10.3969/j.issn.1006-6535.2023.06.019